Formin-mediated nuclear actin assembly at androgen receptors promotes transcriptional droplet formation

Julian Knerr
University of Freiburg https://orcid.org/0000-0002-2614-6185
Ralf Werner
2Division of Pediatric Endocrinology and Diabetes, Department of Pediatrics and Adolescent Medicine, University of Lübeck https://orcid.org/0000-0003-3718-3595
Carsten Schwan
Albert Ludwigs University of Freiburg
Hong Wang
University of Freiburg https://orcid.org/0000-0002-3120-1679
Peter Gebhardt
University of Freiburg
Helga Grötsch
2Division of Pediatric Endocrinology and Diabetes, Department of Pediatrics and Adolescent Medicine, University of Lübeck https://orcid.org/0000-0003-1948-3922
Almuth Caliebe
University Hospitals Schleswig-Holstein https://orcid.org/0000-0003-2157-425X
Malte Spielmann
Institute for Human Genetics, UKSH https://orcid.org/0000-0002-0583-4683
Paul-Martin Holterhus
University Hospital Schleswig-Holstein, Kiel
Robert Grosse (robert.grosse@pharmakol.uni-freiburg.de)
University of Freiburg https://orcid.org/0000-0002-3380-5273
Nadine Hornig (nhornig@medgen.uni-kiel.de)
5Institute of Human Genetics, University Hospital of Schleswig-Holstein https://orcid.org/0000-0003-2469-752X

Biological Sciences - Article

Keywords:

Posted Date: January 31st, 2023

DOI: https://doi.org/10.21203/rs.3.rs-1664650/v1

Version of Record: A version of this preprint was published at Nature on March 27th, 2023. See the published version at https://doi.org/10.1038/s41586-023-05981-1.

Abstract

Steroid hormone receptors are ligand-binding transcription factors essential for mammalian physiology. The androgen receptor (AR) binds androgens mediating gene expression for sexual, somatic, and behavioral functions, and is involved in various conditions including androgen-insensitivity-syndrome (AIS) or prostate cancer. Here we identified functional AIS-patient mutations in the formin and actin nucleator DAAM2. DAAM2 localized to the nucleus and colocalized with the AR to form actin-dependent transcriptional droplets in response to dihydrotestosterone. DAAM2-AR-droplets ranged from 0.02 to 0.06 μm^3 in size and associated with active RNA polymerase II. DAAM2 polymerizes actin directly at the AR to promote droplet fusion in a highly dynamic manner and actin polymerization is required for prostate-specific antigen expression in cancer cells. Our data uncover signal-regulated nuclear actin assembly at a steroid hormone receptor necessary for transcription.

One-sentence Summary

DAAM2 is a candidate gene for partial androgen resistance mediating hormone-induced nuclear actin assembly at AR for transcriptional activity.

Main

Androgen insensitivity syndrome (AIS) is characterized by the inability of the androgen receptor (AR) to respond to androgens resulting in incomplete or absent virilization [1]. Its partial form is characterized by an under-virilized genital phenotype while the complete form is associated with a female appearance despite androgen producing testes. At the molecular level, androgen resistance is caused by hemizygous disrupting mutations in the X-chromosomal androgen receptor (*AR*) gene. While the vast majority of clinically diagnosed complete androgen insensitivity syndromes can be explained by inactivating the *AR* this is true for less than 40% of cases with the clinical diagnosis of partial androgen insensitivity syndrome (PAIS) leaving the majority of these individuals without a clear diagnosis. We previously set up an assay that measures the endogenous AR-activity in its human target tissue, the genital skin fibroblasts (GSFs). This enabled us to identify an *AR*-mutation negative group of AIS characterized by a significant lower AR-activity as compared to male control GSF, named AIS type II [2]. Interestingly, exome sequencing on 26 AIS type II GSF revealed heterozygous variants in the Disheveled-associated activator of morphogenesis 2 (*DAAM2*) gene in two unrelated PAIS individuals born with hypospadias, a micropenis, no Müllerian structures and normal plasma testosterone concentrations (Extended Data Fig. 1a, Extended Data Table 1).

DAAM2 belongs to the formin family of cytoskeletal regulators. Diaphanous-related formins are defined by an N-terminal GTPase-binding-domain (GBD) and formin homology (FH) 1 and 2 domains, which nucleate and polymerize actin [3,4]. Biallelic pathogenic mutations or variants in DAAM2 have been described in steroid-resistant nephrotic syndrome [5]. During mouse embryonic development DAAM2 is expressed in the genital tubercle at embryonal day E14.5, which marks the beginning of the penile

differentiation [6]. In humans, DAAM2 has been proposed as a candidate gene for differences in sex development (DSD) based on a maternally inherited partial duplication of *DAAM2* in a patient with 46, XY DSD and penoscrotal hypospadias [7]. We therefore hypothesized that DAAM2 might be a co-regulator of AR-activity necessary for male genital development.

GSFs from the first patient (GSF-104) harbored a heterozygous frameshift mutation leading to a premature stop codon (p.N614fs*2) thereby yielding a DAAM2 protein lacking the FH2 domain, whereas GSFs from the second patient (GSF-163) revealed a missense mutation in the regulatory GBD (p.D165E) (Extended Data Fig. 1a; Extended Data Table 2). Both GSFs showed a significantly reduced dihydrotestosterone (DHT)-induced AR activity as compared to male control GSFs (Fig. 1a). SiRNA-mediated knock down of DAAM2 in male control GSFs showed a decrease in DHT-induced activation of the AR target gene Apolipoprotein D (*APOD*) (Fig. 1b; Extended Data Fig. 1b, c) indicating a role of DAAM2 in AR activity. Expression analysis of DAAM2 showed reduced expression in mutant GSFs as compared to controls, although only significant at the mRNA level (Extended Data Fig. 1d-h). Cellular fractionation experiments revealed a predominantly nuclear expression of the formin DAAM2 and a reduced nuclear AR signal upon DHT-treatment in both mutant tissues as compared to male control GSFs (Fig. 1c; Extended Data Fig. 1g, h), arguing for a role of nuclear DAAM2 in AR subcellular localization. Notably, formins have been implicated previously in nuclear functions such as transcription, architecture or genome organization [8-12].

Since DAAM2 is a bonafide actin nucleator we tested whether actin associates with the AR. Yeast two-hybrid screening using a cDNA library generated from genital tubercles of male mouse embryos identified several beta actin (*Actb*) clones. Retransformation of the clones with different N-terminally truncated AR fragments revealed that the C-terminal ligand binding domain of the AR was sufficient to bind actin and this interaction was DHT-dependent (Fig. 1d). To further corroborate this finding, we performed actin co-sedimentation assays using purified proteins (Fig. 1e). While no binding was observed in the pellet fraction between F-actin and GST or H2B serving as negative controls (Fig. 1f, g), we observed an association between F-actin and the C-terminal region of AR further confirmed by Western blotting (Fig. 1h) or the C-terminal region of mDia1 (Fig. 1i) serving as a positive control respectively.

Next, we studied the nuclear DAAM2 localization in more detail at the molecular level using lattice structured illumination microscopy (SIM), which allows fast and gentle 3D-superresolution imaging [13-15]. SIM-processing results in an optical resolution of 120 nm in lateral and approximately 400 nm in axial directions. DAAM2 appeared as small spots dispersed in the nuclear compartment (Fig. 2a-c; Extended Data Fig. 2a). These spots increased in total number as well as size upon stimulation with DHT. DHT-induced DAAM2 spots ranged from about 0.02 - 0.06 μm^3 in volume (Fig. 2a, d, e). Interestingly, patient samples harboring mutant DAAM2 did not display DHT-sensitive changes in DAAM2 nuclear spot number or size (Fig. 2b, d, e). DHT-stimulated DAAM2 spots from control cells were sensitive to low concentrations of Hexanediol as well as Swinholide or Latrunculin B treatments (Fig. 2c, d, e), arguing for a role of hydrophobic droplet forming interactions and polymeric actin assembly, respectively. Due to the

shape and Hexanediol sensitivity we refer to these nuclear structures as droplets. Such droplets or clusters have been previously implicated in forming transcriptionally active subcompartments for RNA polymerase II (RNA Pol-II) transcription factory organization [16,17].

Since DAAM2 droplets formed upon testosterone signaling, we asked whether this formin and the AR might colocalize. To reproducibly and quantitatively analyze colocalizations we used an automated threshold [18] validated by comparing droplets with fluorescent beads of 200 nm diameter (Extended Data Fig. 2b, c). DHT-stimulation of control cells resulted in a strong increase of colocalizing AR and DAAM2 positive droplets, while this effect was not observed in DAAM2 mutant patient cells (Fig. 2f, g, j; Extended Data Fig. 2d). Short Hexanediol treatment for 5 minutes completely dissolved colocalization events, which further depended on actin polymerization demonstrated by Swinholide or Latrunculin B addition (Fig. 2h-j; Extended Data Fig. 2d). We also determined the percentage of colocalizing events as compared to total number of DAAM2 droplets confirming a signal-dependent regulation (Extended Data Fig. 2e).

The formin DAAM2 and AR colocalize to form droplet-like assemblies in a signal- as well as actin polymerization-dependent manner. We subsequently investigated whether these droplets associate with active RNA Pol-II to facilitate testosterone-stimulated gene expression. Indeed, stimulation of cells with DHT resulted in colocalization of DAAM2, AR and active RNA Pol-II as indicated by the presence of RNA Pol-II Ser5 phosphorylation (Fig. 3a and b) or RNA Pol-II Ser2 phosphorylation (Extended Data Fig. 2f). We were able to quantify these observations further by measuring the number of events as well as the combined volume of DAAM2 and RNA Pol-II colocalizing with the AR, resulting in an increase of colocalizing events and volume for DAAM2 and RNA Pol-II positive AR-droplets after DHT-signaling compared to control cells over time (Fig. 3e and f). These DHT-triggered colocalizations could not be observed when hydrophobic interactions were blocked by Hexanediol or when actin polymerization was inhibited using Swinholide (Fig. 3d, e, f), suggesting that localized actin assembly promotes transcriptional droplet formation at the AR in a signal-dependent fashion.

To directly test this in living cells we employed a previously characterized tool to visualize endogenous nuclear actin dynamics using a genetically encoded anti-actin chameloid nanobody termed nuclear actin chromobody (nAC) [19-22] and co-expressed AR-GFP in NIH3T3 mouse fibroblasts. We performed live cell superresolution imaging with enhanced temporal resolution by sliding processing (burst mode). The processed videos resulted in a temporal resolution of ~18 frames/s. We visualized AR-displacements of up to 50 nm/frame. Monitoring single AR-droplets over time, we observed striking actin assembly events that directly associated with AR-positive structures. The formation of these actin patches was transient and highly dynamic polymerizing in a range of 1 second, thereby changing their shape and size (Fig. 4a, Extended Data Fig. 3a; Supplementary video 1 and 2). Moreover, we occasionally observed fusion events of two actin-positive AR droplets (Fig. 4b, Supplementary video 3), indicating formation of larger aggregates in an actin-dependent manner. Next, we silenced DAAM2 expression and assessed the percentage of actin-positive AR droplets in living cells. We found a striking DAAM2-dependence for actin assembly at AR droplets demonstrating a tight functional interaction between the formin and nuclear AR droplets (Fig. 4c and d; Extended Data Fig. 3b and c; Supplementary videos 4 and 5).

To this end, we were able to visualize the dynamic interactions as well as actin polymerizing events between DAAM2, the AR and endogenous nuclear actin in real-time (Fig. 4e, Extended Data Fig. 3d; Supplementary videos 6 and 7), thereby revealing direct and spatiotemporally resolved formin-mediated nuclear actin assembly at super-resolution *in vivo* occurring at AR droplets. These actin assembly events appeared to be crucial for AR signaling since the bonafide target gene prostate specific antigen, PSA (also known as kallikrein related peptidase 3, KLK3), was highly sensitive to treatments of Hexanediol or Swinholide (Fig. 4f).

Next, we investigated the impact of nuclear actin assembly for AR transcriptional activity using PSA reporter gene assays. Expression of a nuclear-targeted non-polymerizable actin mutant NLS-R62D or Exportin-6 to reduce nuclear actin levels markedly inhibited DHT-induced AR activity whereas the nuclear-targeted Arp2/3 inhibitory proteins NLS-Arpin or NLS-dominant-negative Arp2 had no effect (Fig. 4g and h, Extended Data Fig. 3e and f). Notably, re-expression of siRNA-resistant DAAM2 partially but significantly rescued DHT-induced AR activity in contrast to mutant DAAM2 (Fig. 4i; Extended Data Fig. 3g-i). Together, our data show that AR signaling depends on DAAM2 and locally defined and highly dynamic nuclear actin polymerization in order to drive transcriptionally active droplet formation.

Conclusions

Here we identified PAIS (AIS type II) patients with mutations in the formin and actin regulator DAAM2 and subsequently uncovered a mechanism by which actin polymerization at a ligand-inducible transcription factor, belonging to the family of steroid hormone receptors, is required for dihydrotestosterone-stimulated AR activity. We found that transient and highly dynamic actin assembly drives AR clustering and droplet formation further undergoing fusion and coalescence events, thereby displaying properties of biomolecular condensates associated with RNA Pol-II transcription [23]. Actin positive AR-droplets coalesce over a distance of 200 to 300 nm within approximately 300 ms, which would be consistent with *in vitro* barbed end actin polymerization rates of roughly 350 monomers/s [24]. Interestingly, actin assembly/disassembly dynamics have been recently implicated to impact the formation and properties of droplet-like structures in an *in vitro* system, supporting the notion that actin filament turnover can be directly involved in the functions of cellular membraneless microcompartments [25]. Our data thus support a model were the AR and actin directly interact, while DAAM2-mediated actin assembly drives AR clustering and droplet formation in response to DHT. Notably, PSA expression in a prostate cancer cell line was sensitive to pharmacological interference with actin assembly as well as condensate formation implicating a potential role for actin-dependent AR transcriptional activity in hormone-sensitive tumor progression. Future studies are needed to address this as well as whether subnuclear actin assembly is involved in the regulation of other ligand-dependent nuclear receptors.

Methods

The study was approved by the Ethical Committee of the Medical Faculty of the Christian-Albrechts-University, Kiel, Germany. When using new samples, starting on 25-06-2014, consent forms were signed

specifically for the current studies (D421/14). We also had access to retrospective samples where patients gave a general consent in order to use clinical data and biomaterial for research on DSD (D401/14). The Ethical Committee approved the use of retrospective samples under the premise of complete anonymization i.e. not having access to any personal data. All GF included in this study were double encrypted. All individuals in the reference group had documented normal male external genitalia.

Cell lines, DNA, plasmids

Genital skin fibroblasts (GSF) GSF-26, GSF-22 (control scrotal cells) and GSF-122, GSF-128 (control foreskin cells) as well as patient cells GSF-104 and GSF-163 were maintained in phenol red free Dulbecco´s modified Eagle´s medium (Life Technologies) supplemented with 10% fetal bovine serum (FBS; Biochrome), 100 units/ml penicillin/streptomycin, 2 mM L-glutamine (Biochrome) and 20 mM HEPES buffer (Life Technologies). NIH3T3 cells were maintained in DMEM (Gibco) supplemented with 10% FCS (ThermoFisher) and 100 units/ml penicillin/streptomycin. LNCaP cells were cultivated in RPMI 1640 media (Gibco) supplemented with 10% fetal bovine serum (Biochrome) and 100 units/ml penicillin/streptomycin (P/S).
DAAM2 wt and N614fs were cloned into pmScarlet backbone by Gibson cloning technique (NEB). The following primers (5´à 3´) were used for cloning of DAAM2-wt-mScarlet:
backbone.rev: ggtggcaagcttgagctcgag; backbone.fwd: ggggatccaatggtgagcaagggcg;
DAAM2.rev: gcctcgcccttgctcaccattggatccccataatttagccggtttattgcccgc;
DAAM2.fwd: ctcgagctcaagcttgccaccatggcccccccgcaagaggag
Following primers were used for Gibson cloning of DAAM2-N614fs-mScarlet plasmid:
backbone.rev: ggtggcaagcttgagctcgag backbone.fwd: ggggatccaatggtgagcaagggcg
N614.fwd: ctcgagctcaagcttgccaccatggcccccccgcaagaggag
N614fs.rev: gcctcgcccttgctcaccattggatcccctgtcagcttcacccagttgaaggacttc
DAAM2-D165E-mScarlet was obtained by a Quick-change PCR of the DAAM2-wt-mScarlet construct with the following forward primer: cggagcatggagcacgccacc
Next, si-DAAM2 (Qiagen, Hs_DAAM2_6 (NM_001201427, NM_015345) binding site gttacccgggagcgggcaataaac was mutated with a Quick change PCR using following primer for DAAM2-wt-mScarlet and DAAM2-D165E-mScarlet to obtain si-resistant DAAM2
plasmids: gttacccgggaacgggcaataaac
Since the shorter frameshift mutant (N614fs-mScarlet) is lacking the binding site (AA1057-1067) for the human si-RNA used in this study, we did not have to modify any si-RNA binding sites for this plasmid.
Arpin ([26]) was amplified with a nuclear localization sequence. Additionally, mScarlet was amplified and both fragments subcloned into pBMN backbone using the following primers via Gibson cloning technique:
mSc_fwd: gatccaccggtcgccaccatggtgagcaagggcgaggcag
mSc_rev: gctcatacaagcttgagctcgagatctgagtccggacttgtac
Arpin_fwd: acaagtccggactcagatctcgagctcaagcttgtatgagc
Arpin-NLS_rev: cactgtgctggcggccgctctatacctttctcttctttttggtccgtcatcccactcctcgtc

pBMN_fwd: agcggccgccagcacagtg
pBMN_rev: ggtggcgaccggtggatccg

NLS-d.n.Arp2 was a gift from O. Fackler [27]

Bacterial protein expression and purification

AR-CT was cloned from pCDNA-AR-CT and inserted into a modified pET-28a plasmid, in which GST was inserted into C-terminus, by Gibson assembly (NEB) using following primers:
AR-CT Fwd: 5'-gtcgacaagattacaaggatgacgatgacaagggaatggaagtgcagttagggctggg-3'
AR-CT Rev: 5'-cgagtgcggccgcaagcctgggtgtggaaatagatgggcttgac-3'
pET-28a Fwd: 5'-gcttgcggccgcactcg-3'
pET-28a Rev: 5'-catccttgtaatcttgtcgacggagctcgaattcggatc-3'
All the plasmids were transformed in *BL21-CodonPlus cell*. Protein expression was induced by adding 1 mM IPTG (Merck) when the absorbance of cell culture reached 0.6-0.8, followed the 16 h incubation at 16℃. After harvesting the cells by centrifugation at 4000 rpm for 20 min, pellet expressing EGFP-H2B or GST was lysed by sonication in TBS buffer (20 mM Tris-HCl, 150 mM NaCl, 1 mM β-Mercaptoethanol) and purified by Protino Ni-IDA Resin (MN)(EGFP-H2B) or Protino Glutathione Agarose 4B (MN) (GST). Pellet expressing AR-CT was lysed by sonication in TEGM (10 mM Tris-HCl, 1 mM EDTA, 10% glycerol, 10 mM molybdate, pH 7.4) and purified by NTA beads. Pellet expressing mDia1-Ct was purified as described in [28].

APOD assay

The assay protocol was published previously [2]. For hormone induction experiments, typically $1.4x10^5$ cells were plated in 60 mm dishes each and incubated at 37°C with 5% CO_2. After 24 h, the dishes were washed three times in the above medium without FBS and were further grown in culture medium supplemented with 0.1% charcoal treated FBS. The dishes were treated as follows: to the first dish non aromatizable DHT (Sigma-Aldrich) dissolved in 100% ethanol was added to a final concentration of 10 nM. An equal volume of ethanol (EtOH) was added to the second dish. Cells were left for 72 h under the above described conditions at 37°C with 5% CO_2 after which they were lysed in RNA-extraction buffer (RLT; Qiagen). DHT was regularly tested for purity and concentration using mass spectrometry.

RNA isolation, amplification and detection

Total RNA was isolated from fibroblasts using the RNeasy kit (Qiagen). Typically, 500 ng of total RNA was reverse transcribed using the QuantiTect Reverse Transcription Kit (Qiagen). Quantitative PCR was performed in duplicate for each sample with the QuantiTect SYBR Green master mix (Qiagen), using specific primers for APOD, DAAM2 and SDHA (succinate dehydrogenase complex flavoprotein subunit A) as a housekeeping gene. All primers were purchased from Qiagen and used following the manufacturer´s

instructions. qPCR data were analyzed using the formula R= 2 – (deltaCP), where R is the relative expression and deltaCP is the difference between APOD or DAAM2 and SDHA expression.

15 x 10^4 LNCaP cells per well were seeded in a 6-well dish in RPMI 1640 media (Gibco) supplemented with 10% fetal bovine serum (Biochrome) and 100 units/ml penicillin/streptomycin (P/S). Non aromatizable DHT (Sigma-Aldrich) dissolved in 100% ethanol was added to a final concentration of 10 nM in RPMI 1640 media supplemented with 10% charcoal stripped FBS (ThermoFisher) and P/S and applied to desired wells. An equal volume of ethanol (EtOH) was added to the control well. 16 h after DHT addition wells were treated with either 5% 1,6-Hexanediol (240117, Sigma-Aldrich) for 5 min at RT or 40 nM Swinholide A (19611, Cayman Chemicals) for 30 min at 37°C, 5% CO_2. After treatments, cells were washed gently with PBS and RPMI 1640 medium with 10% charcoal stripped FBS and DHT or EtOH was added for another 7 hours at 37°C, 5% CO_2. 24h after first DHT addition and treatments in between, cells were lysed in RNA-extraction buffer (RLT; Qiagen).

Total RNA was isolated from LNCaP cells using the RNeasy kit (Qiagen). Following the same methods as described above, specific primers for PSA (prostate specific antigen) and human GAPDH (glyceraldehyde-3-phosphate dehydrogenase) as housekeeping gene were used. Primers were blasted for specificity and purchased from biomers.

RNA interference

3 x 10^4 GSF cells were seeded per 12 well in 12 well dishes in phenol red free Dulbecco´s modified Eagle ´s medium (Life Technologies) supplemented with 10% fetal bovine serum (FBS; Biochrome), 100 units/ml penicillin/streptomycin, 2 mM L-glutamine (Biochrome) and 20 mM HEPES buffer (Life Technologies) and grown at 37°C with 5% CO_2. The next day an siRNA on target plus smart pool against human DAAM2 (L-041010-00-0005; Dharmacon) and an on target plus non-targeting pool (D-001810-10-05, Dharmacon) were added to the cells at a final concentration of 10 nM together with DharmaFECT 1 (T-2001-01; Dharmacon) transfection reagent according to the manufacturer´s instructions. After 24h cells were washed three times in the above medium without FBS and were further grown in culture medium supplemented with 10% charcoal treated FBS and non aromatizable DHT (Sigma-Aldrich) dissolved in 100% ethanol at a final concentration of 10 nM or an equal volume of ethanol (EtOH). Cells were left for 72 h under the above described conditions at 37°C with 5% CO_2 after which they were lysed in RNA-extraction buffer (RLT; Qiagen).

150.000 LNCaP cells/well were seeded in a 12-well plate for Luciferase gene reporter assays and transfected the next day with either 30 pmol control si-RNA (Qiagen), 30 pmol si-RNA directed against human DAAM2 (Qiagen, Hs_DAAM2_6 (NM_001201427, NM_015345) or 30 pmol si-RNA directed against human Diaphanous 3 (Qiagen, Hs_DIAPH3_8; NM_001042517 NM_030932; CTCCGGCACAATTCAGTTCAA) using RNAiMax (Thermofisher). 24h after si-RNA transfection LNCaP were transfected with reporter plasmids as well as DAAM2-rescue plamids and assay was performed 48 h after si-RNA transfection (also see section “PSA-Luciferase gene reporter assay”).

250.000 cells per well NIH/3T3, stably expressing the nuclear actin chromobody-mCherry (nAC-mCherry) were seeded into a 6-well plate. The next day cells were transfected with either 30 pmol control si-RNA or

30 pmol si-RNA directed against mouse Daam2 (Qiagen; Mm_DAAM2_2 NM_001008231) using RNAiMax (ThermoFisher). 24 h after transfection cells were split into 35mm glass bottom dishes (Greiner) and a new 6-well for WB analysis of Daam2-knockdown. Live cell imaging and collection of lysates for WB analysis were performed 72 h after si-RNA transfection (also see section “Microscopy, live imaging and image analysis”).

PSA-luciferase gene reporter assay

300.000 LNCaP wt cells/well were seeded in a 6-well plate in RPMI 1640 media (Gibco) supplemented with 10% fetal bovine serum (Biochrome) and 100 units/ml penicillin/streptomycin (P/S). The next day cells were washed carefully three times with 1x PBS before changing the medium to RPMI 1640 media supplemented with 10% charcoal stripped FBS (ThermoFisher) and P/S. The next day all wells were transfected with 200 ng pRLTK-Renilla-Luc and 400 ng pGL3-PSA-Luc per well using Lipofectamine 3000 (ThermoFisher). Co-transfection of additional plasmids were as followed:

PSA reporter assay NLS-actin R62D: 400 ng NLS-BFP-actin R62D-myc, 800 ng NLS-BFP-actin R62D myc, 400 ng NLS-BFP-myc; control wells: 800 ng pLink each to equal transfected DNA amount.

PSA reporter assay Arp2/3 complex & Exportin-6: 500 ng NLS-Arpin-mScarlet, 500 ng NLS-d.n.Arp 2-mCherry, 300 ng Exportin-6-mCherry; control wells: 500 ng pLink each to equal transfected DNA amount. 5 h after transfection 2 ml of 20 nM DHT in RPMI 1640 media supplemented with 10% charcoal stripped FBS and P/S was added carefully and dropwise to the wells, except one well which was treated with 0.1% Ethanol in RPMI 1640 media supplemented with 10% charcoal stripped FBS and P/S. With the existing 2 ml of RPMI 1640 media supplemented with 10% charcoal stripped FBS (ThermoFisher) and P/S in the wells, we achieved a final concetration of 10 nM DHT in each well. 24 h after DHT addition cells were lysed and assay performed as described below.

For si-RNA based PSA-Luciferase gene reporter assay 150.000 LNCaP wt cells/well were seeded in a 12-well plate. The next day cells were transfected with either 30 pmol control si-RNA (Qiagen), 30 pmol si-RNA directed against human DAAM2 or 30 pmol si-RNA directed against human Diaphanous 3 (see section “RNA interference”) using RNAiMax. 5 h after transfection cells were carefully washed three times with 1x PBS and medium was changed to RPMI 1640 media supplemented with 10% charcoal stripped FBS and P/S. The following morning cells were transfected with reporter plasmids as described above and co-transfected with 500 ng si-RNA resistant DAAM2-wt-mScarlet, DAAM2-D165E-mScarlet or DAAM2-N614fs-mScarlet plasmids. Control wells and si-DIAPH3 treated wells were transfected with 500 ng pLink each to reach equal DNA amounts in all wells. 5 h after transfection 1 ml of 20 nM DHT in RPMI 1640 media supplemented with 10% charcoal stripped FBS and P/S was added carefully and dropwise to the wells, except one well which was treated with 0.1% Ethanol in RPMI 1640 media supplemented with 10% charcoal stripped FBS and P/S. With the existing 1 ml of RPMI 1640 media supplemented with 10% charcoal stripped FBS (ThermoFisher) and P/S in the wells, we achieved a final concetration of 10 nM DHT in each well. 24 h after DHT addition medium was aspirated and cells were lysed in 200 µl (6-well) or

100 µl (12-well) Triton lysis buffer (0.15 M Tris, 75 mM NaCl, 3 mM $MgCl_2$, 0.25% Triton X-100) for 10 min on ice with occasional shaking. Cells were scraped and centrifuged at full speed and 4°C for 10 min. 20 µl of each lysate were pipetted into a 96-well plate. 50 µl of firefly buffer (15 mM DTT, 0.6 mM coenzyme A, 0.45 mM ATP, 4.2 mg/ml D-luciferin) was added simultaneously into the lysates and luminescence was measured after 10 seconds. Following 75 µl of renilla buffer (45 Mm EDTA, 30 mM $Na_4P_2O_7$, 1.425 M NaCl, 0.06 mM PTC124, 0.01 h-CTZ) were added to stop the reaction and luminescence was measured again. Afterwards, final luciferase values were determined with the following equation and normalized to the ethanol control:

$$\frac{pGL3\ PSA - Luc}{pRLTK\ Renilla - Luc} = final\ Luciferase\ value$$

Afterwards 5x Laemmli sample buffer was added to the lysates, heated up at 95°C for 10 min, centrifuged for 3 min and conducted to WB analysis. Protein expression and knockdown efficiency were detected using following primary antibodies: anti-myc (CST, 2272S); anti-Histone H3 (CST, 4499S); anti-mCherry (CST, ED8F), anti-RFP (Rockland, 600401379); anti-GAPDH (Millipore, 3587127); anti-alpha tubulin (CST, 2125S); anti-DAAM2 (abcam, ab169527) & anti DIAPH3 (proteintech, 14342-1-AP).

Whole cell protein extracts, biochemical fractionation and protein detection

For protein extractions GSF cells were grown in phenol red free Dulbecco´s modified Eagle´s medium (Life Technologies) supplemented with 10% fetal bovine serum (FBS; Biochrome), 100 units/ml penicillin/streptomycin, 2 mM L-glutamine (Biochrome) and 20 mM HEPES buffer (Life Technologies) at 37°C with 5% CO_2 to a confluence of 70-80%. For whole cell extracts, cells were washed once in ice-cold PBS, resuspended in ice-cold RIPA buffer supplemented with complete protease inhibitors (Complete™ Roche). After 10 minutes centrifugation at 15.000 g and 4°C, the supernatant was transferred into a fresh tube and snap frozen on dry ice. For biochemical fractionation, cells were washed three times in the above medium without FBS and were further grown in culture medium supplemented with 10% charcoal treated FBS. Cells were treated with non aromatizable DHT (Sigma-Aldrich) dissolved in 100% ethanol at a final concentration of 10 nM or an equal volume of ethanol (EtOH). Cells were left for 48 h under the above described conditions at 37°C with 5% CO_2. Protein fractionation was performed as described before [19]. Cells were washed with ice cold phosphate-buffered saline (PBS), scraped in ice cold PBS and centrifuged for 10 min at 800g. The pellet was kept on dry ice for 45 min after which it was dissolved in 5x volume of buffer P1 (10mM HEPES, 0.1mM EGTA, 1mM DTT, complete protease inhibitors (Complete™ Roche)) and kept for 10 min on ice. After addition of Triton X-100 (final concentration 0.5%), samples were vortexed for 10 s, followed by the sedimentation of the nuclei at 10,000g for 10 min. The supernatant was kept at -80°C as cytoplasmic fraction. The pellet was washed twice with buffer P1 and lysed in 5 x volume of buffer P2 (20 mM HEPES, 25% glycerol, 400 mM NaCl, 1 mM EGTA, 1 mM DTT, complete protease inhibitors (Complete™ Roche)) for 90 min on a rotary shaker at 4°C followed by 30

min centrifugation at 16,000 g. The supernatant was kept at -80°C as nuclear fraction. Protein extracts were separated by SDS-PAGE on a NuPAGE® Novex® 4-12% Bis-Tris Protein gel (Life Technologies) and transferred to a nitrocellulose membrane (Whatman, GE Healtehcare Life Sciences). The membrane was blocked for 1-2 h at room temperature with TBS containing 0.1% Tween and 5% non-fat dry milk. All primary antibodies were used over night at 4°C: Anti-AR F39.4.1 antibody (BioGenex) (1:100 dilution), Anti-Actin (A 2066) antibody (Sigma-Aldrich) (1:10.000 dilution), Anti-DAAM2 antibody (ab169527, abcam) (1:1.000 dilution), Anti-TAF15 antibody (ab134916, abcam) (1:10.000 dilution), Anti-TUB antibody (T5168, sigma) (1:10.000 dilution). Secondary anti-rabbit and anti-mouse antibodies (Immuno Reagents Inc.) were incubated for 1-2 h at room temperature (1:4.000 dilution). All antibodies were resuspended in TBS containing 0.1% Tween and 5% non-fat dry milk. Signals were detected with the Biorad Chemidoc imaging system using the Clarity Max Western ECL Substrate (Biorad). Quantification of signals was performed using the Image Lab software 6.0.1 (Biorad Technologies).

Yeast two hybrid

Yeast two hybrid screening was performed as described previously [29]. In brief, RNA of male mouse genital tubercles at the beginning of external genital development at embryonic day 15 and 16 (E15, screening A/ E16, screening B) were extracted. Independent cDNA libraries of each embryonic day were constructed using the Matchmaker Library Construction and Screening Kit (Clontech) and fused to the GAL4-AD in pGADT7-Rec by cotransfection into the yeast strain AH109. Vector pGBKT7-AR555 containing the C-terminal part of the AR (amino acid 555-920) containing the DNA-binding domain (DBD), hinge region and ligand binding domain (LBD) was used as a bait. Plasmids of colonies grown after 3-5 days at 30°C were recovered and inserts of pGADT7-Rec were identified by sequencing. AR-binding of fusion proteins of purified plasmids was verified by retransformation into yeast strain AH109 together with the bait used in the screening or with pGBKT7-AR645 containing a shortened AR-bait containing only the ligand binding domain (LBD, aa 645-920). The empty pGBKT7 vector was used as a negative control.

In-vitro Co-sedimentation assay

In order to identify whether the purified c-terminal Androgen receptor protein (AR-Ct-GST) directly binds to F-actin, G-actin (10 µM, Cytoskeleton Inc.) was incubated with either purified AR-Ct-GST (15 µM), mDia1-Ct (5 µM), GST (5 µM) or EGFP-H2B (5 µM) for 1 h at room temperature in F-buffer (5 mM Tris-HCl pH 7.5, 100 mM KCl, 1 mM $MgCl_2$, 0.2 mM $CaCl_2$, 0.2 mM EGTA, 0.2 mM ATP and 0.5 mM DTT) with a total volume of 100 µl. GST, as well as EGFP-H2B were used as negative controls whereas mDia1-Ct was used as the positive control sample. After ultracentrifugation at 80.000 g for 30 min, 96 µl supernatant was removed as the nonpelleted fraction (S) and boiled in 24 µl 5X Laemmli buffer. The pellet (P) was washed one time with F-buffer, then resuspended and boiled in 120 µl 1X Laemmli buffer. 20 µl of each sample was loaded into the SDS-PAGE gel. Furthermore, the same lysates from the aforementioned AR-Ct-GST experiment were subjected to Western Blot analysis and incubated with an antibody recognizing the c-terminus of the AR (Androgen receptor antibody C-terminal antigen; Cellsignaling #54653S).

Immunofluorescence

6 x 10^4 cells were seeded per 6 wells in 6-well dishes in phenol red free Dulbecco´s modified Eagle´s medium (Life Technologies) supplemented with 10% fetal bovine serum (FBS; Biochrome), 100 units/ml penicillin/streptomycin, 2 mM L-glutamine (Biochrome) and 20 mM HEPES buffer (Life Technologies) and grown at 37°C with 5% CO_2. After 24 h cells were washed three times in the above medium without FBS and were further grown in culture medium supplemented with 10% charcoal treated FBS and non aromatizable DHT (Sigma-Aldrich) dissolved in 100% ethanol at a final concentration of 10 nM or an equal volume of ethanol (EtOH). Cells were left for 24 h under the above described conditions at 37°C with 5% CO_2. For Swinholide A (19611, Cayman Chemicals) treatment a final concentration of 40 nM in culture medium supplemented with 10% charcoal treated FBS was used and left for 30 min at 37°C with 5% CO_2. 1,6-Hexanediol (240117, Sigma-Aldrich) was used at a final concentration of 5% in culture medium supplemented with 10% charcoal treated FBS and left for 5 min at room temperature. Cells were washed subsequently with PBS and fixed 10 min in 4% formaldehyde solution (28906, Thermo Fisher Scientific) at room temperature. Formaldehyde was washed out with PBS and cells were blocked for 1 h with 2% BSA () and 0.2% Triton X-100 () at room temperature. Cells were washed again with PBS before adding primary antibodies diluted in 2% BSA and 0.2% Triton X-100: Anti-AR F39.4.1 (BioGenex) (1:100), Anti-DAAM2 (ab169527, abcam) (1:100), Anti-RNA Pol II CTD phospho Ser5 (61986, Active Motif) (1:300), Anti-RNA polymerase II CTD repeat YSPTSPS (Ser2P) (ab193468, abcam) and left for 1-2 h at room temperature in a humid chamber. Cells were washed 5x with PBS before adding the fluorescent labeled secondary antibodies diluted in 2% BSA and 0.2% Triton X-100: Alexa Fluor 594 goat anti-mouse IgG(H+L) (A-11005, Thermo Fisher Scientific) (1:500), Alexa Fluor 488 goat anti-rabbit IgG(H+L) (A-11008, Thermo Fisher Scientific) (1:500), Alexa Fluor 647 goat anti-Rat IgG (H+L) (A-21247, Thermo Fisher Scientific) (1:400) and left for 1 h at room temperature in a dark humid chamber. Cells were washed 3x with 0.1% Tween 20 in PBS, 1x with PBS and 1x with distilled water. Cells were mounted with 1.5 µg/ml DAPI in antifade mounting medium (Vectashield H-1000, Biozol).

Microscopy, live imaging and image analysis

Images were generated using ELYRA7, structured-illumination-microscropy with 3D Lattice SIM (Zeiss), equipped with a 63x 1,4 Oil DIC objective, Pecon incubation chamber ensuring 37°C and 5% CO_2 and processed using Zen black software (Zeiss). For SIM reconstruction the theoretical OTF given by the manufacturer was used and the automated Wiener-Filter-strength given by the “Standard” end-criterion of the manufacturer was applied. Thus, Values for Wiener-Filter varied closely around $10^{(-10)}$ for all samples and in all channels. Baseline-shift was used for all reconstructed images as a standard. Thus, the threshold was set into the appearing first peak in the histogram for representative images but no grey-values of the histogram were influenced or cut off for further quantitative analysis. Maximum resolution enhancement by minimal artifact structure (honeycomb-interferences with the sample) was targeted. This was achieved by constantly using “baseline-shift” method and comparing background patterns with structure-signals.

For 3D-reconstruction of droplets and 3D-colocalization quantifications, cells were treated and stained as indicated and imaged as z-stack with 0.091 µm interval. Each z-stack was processed using Imaris software 64x 9.9.0 and displayed as maximum intensity projection (MIP). Droplet size was quantified in Imaris, enabling detection of number and size of single droplets in the nucleus. For quantification of DAAM2 droplet volumes, we excluded droplets smaller than 0.0185 μm^3 due to limitation in z-resolution. Brightness and contrast were applied equally to all images, prior to quantification.
For 3D-colocalization between AR and DAAM2 we used the “Coloc-Tool” of Imaris identifying double positive voxels. Thresholds for the analyzed channels were determined in DHT-treated cells by the 'Calculate Thresholds' function in the Imaris- Coloc-tool and applied to all other images equally. This function is based on the algorithm by [18] which has been commercialized by Bitplane AG (Zurich, Switzerland). As a variation to the published algorithm the sample distribution of the Pearson's ”*r*” was differently randomized. Sample distribution was approximated by Gaussian distribution with a mean of 0 and a variance of n/N with n= number of voxels in the point spread function (PSF) and N = number of all voxels. Following, a new colocalization-channel was generated and 3D rendered by Imaris. Numbers, as well as volumes were quantified using the “surface tool” of Imaris.
For 3D-colocalization between DAAM2 and RNA Pol-II together with the AR, threshold between DAAM2 and RNA Pol-II was determined again using the 'Calculate Thresholds' function' and applied to all images. A fluorescence-based mask was used to set the region of interest (ROI) for the AR, thereby just detecting overlapping fluorescence of DAAM2 and RNA Pol-II in this ROI. Following, a new colocalization-channel was generated and 3D rendered by Imaris. Further analyzation for numbers, as well as volumes, was performed using the “surface tool” of Imaris and displayed as volume heat maps.
For live cell imaging NIH3T3, stably expressing nuclear actin chromobody-mCherry (nAC-mCherry), were seeded in DMEM (Gibco) supplemented with 10% FCS and P/S in a 6-well (Greiner) at 37°C and 5% CO_2. The next day 30 pmol of control si-RNA and si-DAAM2 (Qiagen; Mm_DAAM2_2 NM_001008231) were transfected. 24 h after transfection cells were split into 35mm glass bottom dishes (Greiner). 48 h after si-RNA transfection 500 ng of AR-GFP in Opti-MEM (ThermoFisher) were transfected using FuGENE (Promega), following manufacturer’s instructions. 5 h after transfection, medium was changed to 10 nM DHT in DMEM supplemented with 10% charcoal stripped FCS and P/S. 72 h after si-RNA transfection and 16h after addition of DHT imaging was performed. For quantification of actin positive AR droplets, videos were processed using sliding processing (Burst-mode, Zeiss) and first timepoint of each video was analyzed. Using the “spots tool” of Imaris, actin and AR droplets were detected independently as single spots. Following, all actin spots within 100 nm proximity from the center of AR spots were filtered and assigned as actin-positive AR droplets and plotted as percentage of total AR droplets.
LNCaP cells were seeded in RPMI 1640 media (Gibco) supplemented with 10% fetal bovine serum (Biochrome) and 100 units/ml penicillin/streptomycin (P/S) in a glass bottom dish (Greiner). The next day, cells were transfected with AR-GFP, DAAM2-mScarlet and nuclear actin chromobody-SNAP (nAC-SNAP) using Lipofectamine 3000, following manufacturer´s instructions. 5 h after transfection medium was changed to RPMI 1640 media supplemented with 10% charcoal stripped FBS (ThermoFisher) and P/S as well as 10 nM DHT. 30 min prior to imaging SNAP-cell 647-SiR (NEB) was added to label SNAP-tag. Live cell videos were acquired as single plane videos with the minimal time interval and further

processed using sliding processing (Burst-mode, Zeiss) resulting in a temporal resolution of 18 frames/second.

Next generation sequencing library preparation and sequencing

For exome sequencing, a sequencing library was created using Sure Select Human All Exon V6 technology (Agilent) and sequencing was performed at the Cologne Center of Genomics (CCG) on an Illumina platform with paired-end sequencing at a read length of 150 nucleotides. On average, 86% of the target regions were covered 30x and 97% of the target regions were covered 10x. The sequencing data were annotated and quality-checked according to an in-house pipeline and evaluated using the varbank software (CCG) (https://varbank.ccg.uni-koeln.de/). The following filters were used for the evaluation: exclusion of low complexity regions, maximum allele frequency of 0.01% according to gnomAD (https://gnomad.broadinstitute.org), maximum in-house allele frequency of 0.1%, minimum 6-fold coverage. Candidate genes were checked in the UCSC browser for their conservation and the CADD score (Combined Annotation Dependent Depletion) [30].

First, the sequencing data were analyzed separately and checked for homozygous, hemizygous and possible compound heterozygous changes. This resulted in a number of 10-30 changes per patient. These were checked again for their sequencing quality. All genes were subjected to a literature search. For this purpose, search terms for the respective candidate gene were entered separately in PubMed-NCBI and in the Cardiff Human Gene Mutation Database in connection with sex development in general and androgen resistance or androgen receptor in particular, and positive hits were tabulated. This reduced the number of the candidate genes to 1-3 per patient. Due to their high number, heterozygous sequencing variants were specifically screened for known DSD genes. A list of the known DSD genes was compiled from publications [31,32]. In parallel, all samples were analyzed simultaneously and subjected to a phenotype-ontology analysis. The web tool Phenomizer was used for this [33]. PAIS (ORPHA:90797) was used as the Human Phenotype Ontology (HPO) term because all included patients had a clinical diagnosis of partial androgen resistance.

Sanger sequencing of the AR was performed on the ABI 3130 Genetic Analyzer (Applied Biosystems).

Statistics

Statistical analysis was performed using Graph Pad 9.3. Data are presented as column bar graph ± SD, scatter dot bar plot with mean ± SD or violin plots showing all data points with median and quartiles. Statistical significance was evaluated with one-way ANOVA for multiple comparisons. For comparison of two groups data two-tailed *t*-test was used, when data were normally distributed. If data were not normally distributed a Mann-Whitney *t*-test was performed. Statistical significance is indicated as *p < 0.05, **p < 0.01, ***p < 0.001, and ****p < 0.0001.

Declarations

Data availability

“All data are available in the main text or the supplementary materials.”

Acknowledgments

We thank B. Karwelies and P. Davarnia for technical support. We thank laboratory members of the Grosse group for discussions and O. Wunderlich for technical assistance and J. Altmueller for help with the sequencing facility. We are grateful to H.U. Schweikert for providing GSFs. We would like to thank the referees for their helpful and constructive criticism.

Funding

The study has been funded by the German Research Council (Deutsche Forschungsgemeinschaft, DFG) to NCH (HO 6028/2-1), as well as to RG (GR2111/13-1) and under Germany's Excellence Strategy (EXC-2189, project ID: 390939984).

Author information

Authors and affiliations

Contributions

Conceptualization: NCH, RG

Methodology: NCH, RG, JK, RW, HG, HW, PG, CS

Visualization: NCH, JK, RW, CS

Funding acquisition: NCH, RG

Project administration: NCH, RG

Supervision: NCH, RG

Writing – original draft: NCH, RG

Writing – review & editing: RW, AC, MS, PMH

Ethics declaration

“Authors declare that they have no competing interests.”

References

1. Hornig, N. C. & Holterhus, P. M. Molecular basis of androgen insensitivity syndromes. *Mol Cell Endocrinol***523**, 111146 (2021). https://doi.org:10.1016/j.mce.2020.111146
2. Hornig, N. C. *et al.* Identification of an AR Mutation-Negative Class of Androgen Insensitivity by Determining Endogenous AR Activity. *J Clin Endocrinol Metab***101**, 4468-4477 (2016). https://doi.org:10.1210/jc.2016-1990
3. Faix, J. & Grosse, R. Staying in shape with formins. *Dev Cell***10**, 693-706 (2006). https://doi.org:10.1016/j.devcel.2006.05.001
4. Goode, B. L. & Eck, M. J. Mechanism and function of formins in the control of actin assembly. *Annu Rev Biochem***76**, 593-627 (2007). https://doi.org:10.1146/annurev.biochem.75.103004.142647
5. Schneider, R. *et al.* DAAM2 Variants Cause Nephrotic Syndrome via Actin Dysregulation. *Am J Hum Genet***107**, 1113-1128 (2020). https://doi.org:10.1016/j.ajhg.2020.11.008
6. Nakaya, M. A. *et al.* Identification and comparative expression analyses of Daam genes in mouse and Xenopus. *Gene Expr Patterns***5**, 97-105 (2004). https://doi.org:10.1016/j.modgep.2004.06.001
7. Calvel, P. *et al.* A Case of Wiedemann-Steiner Syndrome Associated with a 46,XY Disorder of Sexual Development and Gonadal Dysgenesis. *Sex Dev***9**, 289-295 (2015). https://doi.org:10.1159/000441512
8. Baarlink, C., Wang, H. & Grosse, R. Nuclear actin network assembly by formins regulates the SRF coactivator MAL. *Science***340**, 864-867 (2013). https://doi.org:10.1126/science.1235038
9. Wang, Y. *et al.* GPCR-induced calcium transients trigger nuclear actin assembly for chromatin dynamics. *Nature Communications***10**, 1-9 (2019). https://doi.org:10.1038/s41467-019-13322-y
10. Belin, B. J., Lee, T. & Mullins, R. D. DNA damage induces nuclear actin filament assembly by formin-2 and spire-1/2 that promotes efficient DNA repair. *eLife***4**, 1-21 (2015). https://doi.org:10.7554/eLife.07735
11. Liu, C., Zhu, R. & Mao, Y. Nuclear Actin Polymerized by mDia2 Confines Centromere Movement during CENP-A Loading. *iScience***9**, 314-327 (2018). https://doi.org:10.1016/j.isci.2018.10.031
12. Aymard, F. *et al.* Genome-wide mapping of long-range contacts unveils clustering of DNA double-strand breaks at damaged active genes. *Nat Struct Mol Biol***24**, 353-361 (2017). https://doi.org:10.1038/nsmb.3387
13. Betzig, E. Excitation strategies for optical lattice microscopy. *Opt Express***13**, 3021-3036 (2005). https://doi.org:10.1364/opex.13.003021
14. Heintzmann, R. Saturated patterned excitation microscopy with two-dimensional excitation patterns. *Micron***34**, 283-291 (2003). https://doi.org:10.1016/s0968-4328(03)00053-2

15. Gustafsson, M. G. Surpassing the lateral resolution limit by a factor of two using structured illumination microscopy. *J Microsc***198**, 82-87 (2000). https://doi.org:10.1046/j.1365-2818.2000.00710.x
16. Rippe, K. & Papantonis, A. Functional organization of RNA polymerase II in nuclear subcompartments. *Current Opinion in Cell Biology***74**, 88-96 (2022). https://doi.org:10.1016/j.ceb.2022.01.005
17. Boehning, M. *et al.* RNA polymerase II clustering through carboxy-terminal domain phase separation. *Nat Struct Mol Biol***25**, 833-840 (2018). https://doi.org:10.1038/s41594-018-0112-y
18. Costes, S. V. *et al.* Automatic and quantitative measurement of protein-protein colocalization in live cells. *Biophys J***86**, 3993-4003 (2004). https://doi.org:10.1529/biophysj.103.038422
19. Baarlink, C. *et al.* A transient pool of nuclear F-actin at mitotic exit controls chromatin organization. *Nature Cell Biology***19**, 1389-1399 (2017). https://doi.org:10.1038/ncb3641
20. Plessner, M., Melak, M., Chinchilla, P., Baarlink, C. & Grosse, R. Nuclear F-actin formation and reorganization upon cell spreading. *Journal of Biological Chemistry***290**, 11209-11216 (2015). https://doi.org:10.1074/jbc.M114.627166
21. Caridi, C. P. *et al.* Nuclear F-actin and myosins drive relocalization of heterochromatic breaks. *Nature***559**, 54-60 (2018). https://doi.org:10.1038/s41586-018-0242-8
22. Schrank, B. R. *et al.* Nuclear ARP2/3 drives DNA break clustering for homology-directed repair. *Nature***559**, 61-66 (2018). https://doi.org:10.1038/s41586-018-0237-5
23. Cho, W. K. *et al.* Mediator and RNA polymerase II clusters associate in transcription-dependent condensates. *Science***361**, 412-415 (2018). https://doi.org:10.1126/science.aar4199
24. Funk, J. *et al.* Profilin and formin constitute a pacemaker system for robust actin filament growth. *eLife***8**, 1-34 (2019). https://doi.org:10.7554/eLife.50963
25. Waizumi, T. *et al.* Polymerization/depolymerization of actin cooperates with the morphology and stability of cell-sized droplets generated in a polymer solution under a depletion effect. *J Chem Phys***155**, 075101 (2021). https://doi.org:10.1063/5.0055460
26. Plessner, M., Knerr, J. & Grosse, R. Centrosomal Actin Assembly Is Required for Proper Mitotic Spindle Formation and Chromosome Congression. *iScience***15**, 274-281 (2019). https://doi.org:10.1016/j.isci.2019.04.022
27. Tsopoulidis, N. *et al.* T cell receptor–triggered nuclear actin network formation drives CD4+ T cell effector functions. *Science Immunology***4** (2019). https://doi.org:10.1126/sciimmunol.aav1987
28. Li, F. & Higgs, H. N. The mouse Formin mDia1 is a potent actin nucleation factor regulated by autoinhibition. *Curr Biol***13**, 1335-1340 (2003). https://doi.org:10.1016/s0960-9822(03)00540-2
29. Grotsch, H. *et al.* RWDD1 interacts with the ligand binding domain of the androgen receptor and acts as a coactivator of androgen-dependent transactivation. *Mol Cell Endocrinol***358**, 53-62 (2012). https://doi.org:10.1016/j.mce.2012.02.020

30. Teotonio, H., Chelo, I. M., Bradic, M., Rose, M. R. & Long, A. D. Experimental evolution reveals natural selection on standing genetic variation. *Nat Genet***41**, 251-257 (2009). https://doi.org:10.1038/ng.289
31. Eggers, S. *et al.* Disorders of sex development: insights from targeted gene sequencing of a large international patient cohort. *Genome Biol***17**, 243 (2016). https://doi.org:10.1186/s13059-016-1105-y
32. Audi, L. *et al.* GENETICS IN ENDOCRINOLOGY: Approaches to molecular genetic diagnosis in the management of differences/disorders of sex development (DSD): position paper of EU COST Action BM 1303 'DSDnet'. *Eur J Endocrinol***179**, R197-R206 (2018). https://doi.org:10.1530/EJE-18-0256
33. Ullah, M. Z., Aono, M. & Seddiqui, M. H. Estimating a ranked list of human hereditary diseases for clinical phenotypes by using weighted bipartite network. *Annu Int Conf IEEE Eng Med Biol Soc***2013**, 3475-3478 (2013). https://doi.org:10.1109/EMBC.2013.6610290

Figures

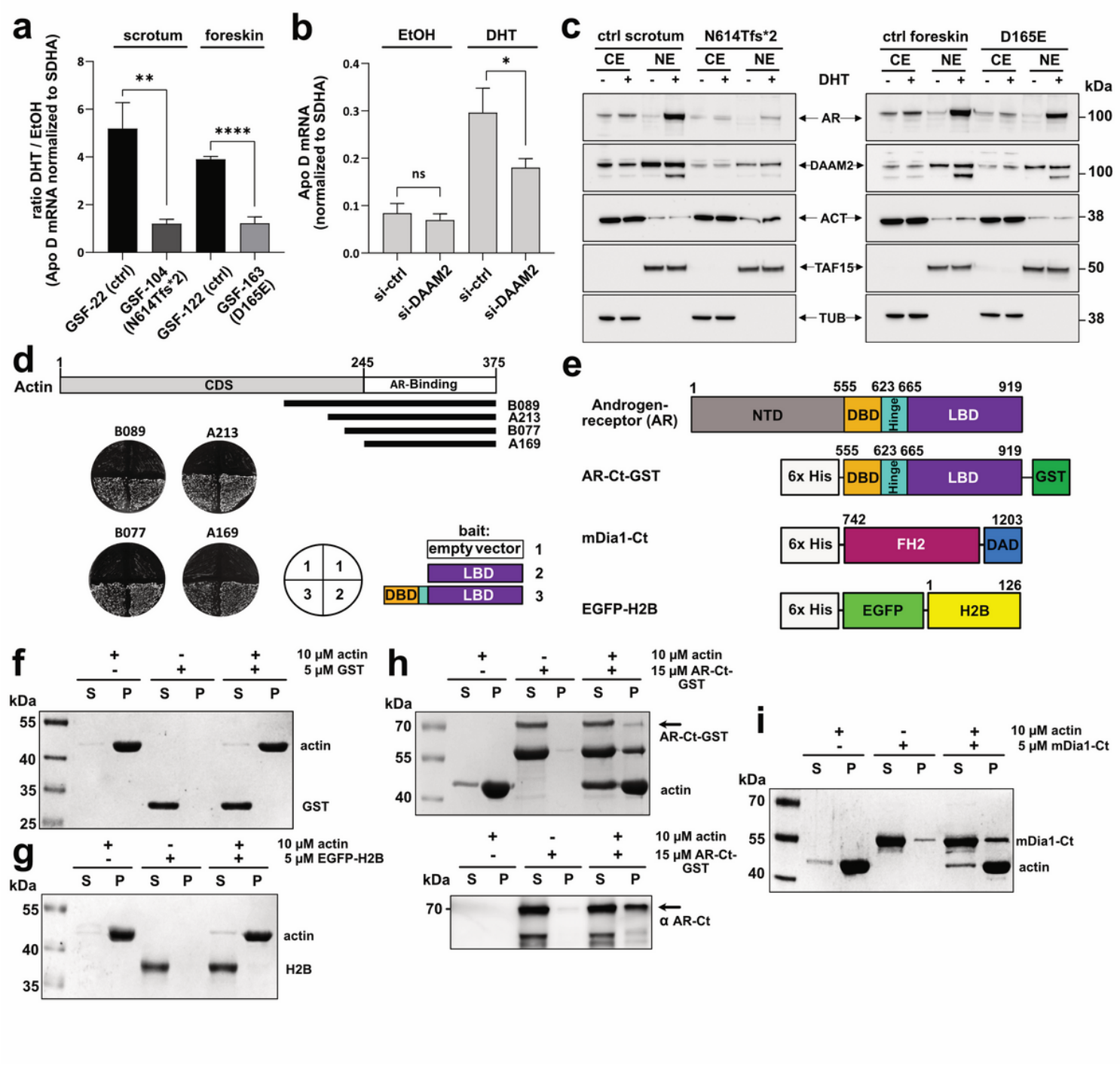

Figure 1

AR activity requires DAAM2 and the AR C-terminus associates with F-actin. a DHT-dependent, AR-induced *APOD* mRNA expression represented as the ratio between ethanol (EtOH)- and DHT-treated patient derived GSFs as compared to tissue specific male control GSFs in 3 independent biological replicates. **b** siRNA mediated knock-down of *DAAM2* in male control GSF. **c** Cytoplasmic (CE) and nuclear (NE) expression of AR, DAAM2 and ACT in male control GSF (GSF-26 and GSF-128) and both mutant strains. TAF15 and TUB served as compartment specific loading controls. **d** Schematic representation of four independent *Actb* cDNA clones (B089, A213, B077, A169) identified using two independent yeast two-hybrid libraries (A, B) derived from RNA of male mouse genitalia development at embryonic days E15 (A) and E16 (B)

(upper panel). C-terminal constructs of the AR were used as bait in the presence of 100 nM DHT. Agar plates show retransformation of the four actin clones in presence of 100 nM DHT with the AR-bait used in the screening (2 and 3). The empty vector (1) served as ~~a~~ negative control. DBD: DNA-binding domain (orange), Hinge (cyan); LBD: ligand binding domain (purple). **e** Cartoon illustrating functional domains of purified proteins used for Co-sedimentation assays. **f-i** SDS-gels of F-actin Co-sedimentation assay of GST (**f**), EGFP-H2B (**g**), AR-Ct-GST (**h**, upper panel; corresponding WB from same lysate, **h** lower panel) and mDia1-Ct (**i**); S represents non-pelleted fraction; P represents pelleted fraction containing F-actin.

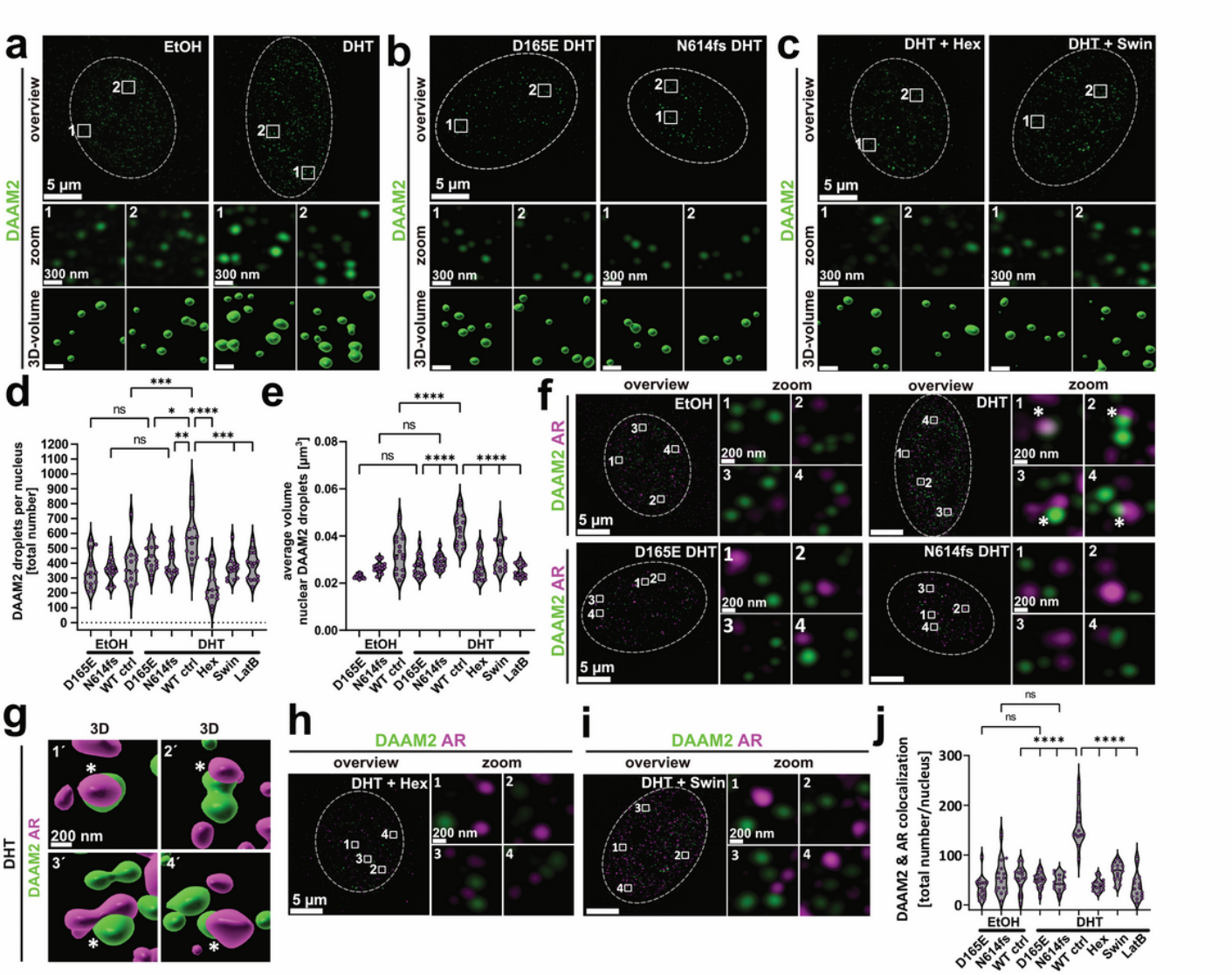

Figure 2

Endogenous nuclear DAAM2 droplet formation and volume is dependent on DHT signaling in control cells and colocalize with endogenous AR. a-c Immunofluorescence (IF) of endogenous DAAM2 (green) in control scrotal cells (**a**), in AIS-patient cells (D165E, N614fs) treated with EtOH or DHT (**b**), and in DHT-

treated control scrotal cells upon addition of Hexanediol or Swinholide (**c**); areas of zoom images are indicated above. Lower panel represents 3D-volume rendering of DAAM2 IF; scale bar overview: 5 µm; zoom: 300 nm; 3D-surface: 300 nm (**a-c**). **d** Quantification of total DAAM2 droplet number per nucleus. **e** Quantification of average DAAM2 droplet volume per nucleus. **f** IF of endogenous DAAM2 (green) and AR (magenta) in control scrotal cells upon stimulation with EtOH or DHT; colocalization is indicated by white asterisks. **g** Corresponding 3D-volume rendering of DAAM2 and AR IF-Signal in (**f**) for DHT-treated control cells. **h-i** IF of endogenous DAAM2 (green) and AR (magenta) in AIS-patient cells (D165E, N614fs) upon stimulation with EtOH or DHT (**h**) or in DHT-treated control scrotal cells upon addition of Hexanediol or Swinholide (**i**). **j** Quantification of total colocalization events between DAAM2 and AR. Data of 15 cells per treatment displayed as violin plot showing all data points with median and quartiles in 3 independent biological replicates (**d**, **e**, **j**). All images are shown as maximum intensity projection; nucleus is indicated by white dashed line from DAPI channel (not shown).

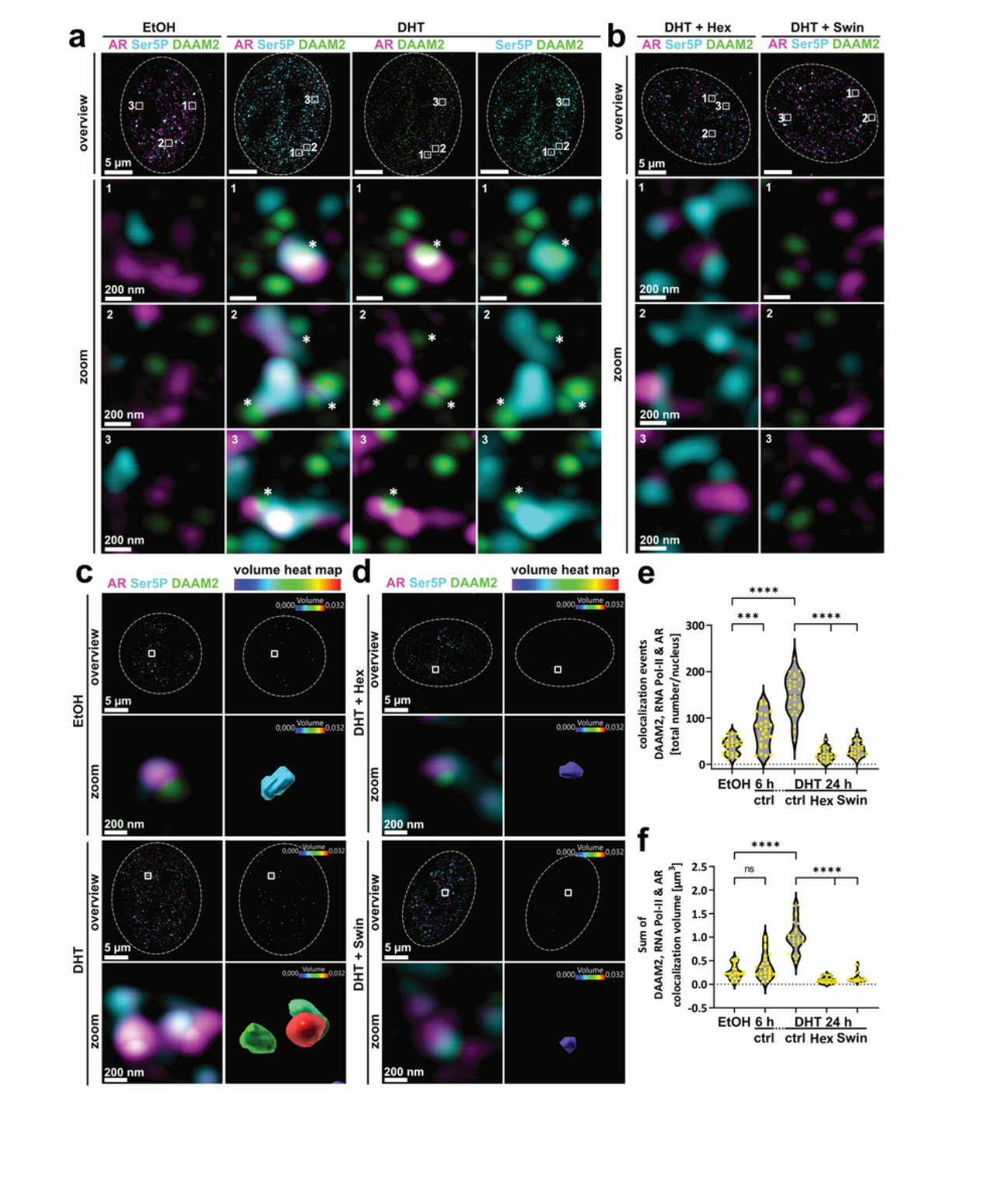

Figure 3

Endogenous DAAM2, AR and active RNA Polymerase-II colocalize actin-dependent upon DHT stimulation in control cells. a IF of endogenous DAAM2 (green), AR (magenta) and active RNA Pol-II (Ser5P, cyan) in control scrotal cells upon stimulation with EtOH or DHT; nucleus is indicated by white dashed line; areas of zoom images are indicated; colocalization events are marked with white asterisks. Scale bar overview: 5 µm; zoom: 200 nm**. b** Immunofluorescence of endogenous DAAM2 (green), AR (magenta) and active

RNA Pol-II (Ser5P, cyan) in control scrotal cells upon treatment with Hexanediol or Swinholide; areas of zoom are indicated; scale bar overview: 5 µm; zoom: 200 nm. **c** 3D-volume rendering of combined colocalization between DAAM2 and RNA Pol-II with the AR for EtOH and DHT-treated control cells; colocalization is displayed as volume heat map. Blue colour code resembles smaller volumes, whereas a red colour code resembles bigger volumes. **d** 3D-volume rendering of combined colocalization between DAAM2 and RNA Pol-II at the AR for DHT-treated control cells, after addition of Hexanediol or Swinholide; colocalization is displayed as volume heat map. **e** Quantification of colocalizing events per nucleus between DAAM2 and RNA Pol-II at the AR. **f** Quantification of colocalizing volumes of DAAM2 and RNA Pol-II with AR. Data of 25 cells per treatment displayed as violin plot showing all data points with median and quartiles in 3 independent biological replicates. All images are shown as Maximum intensity projection.

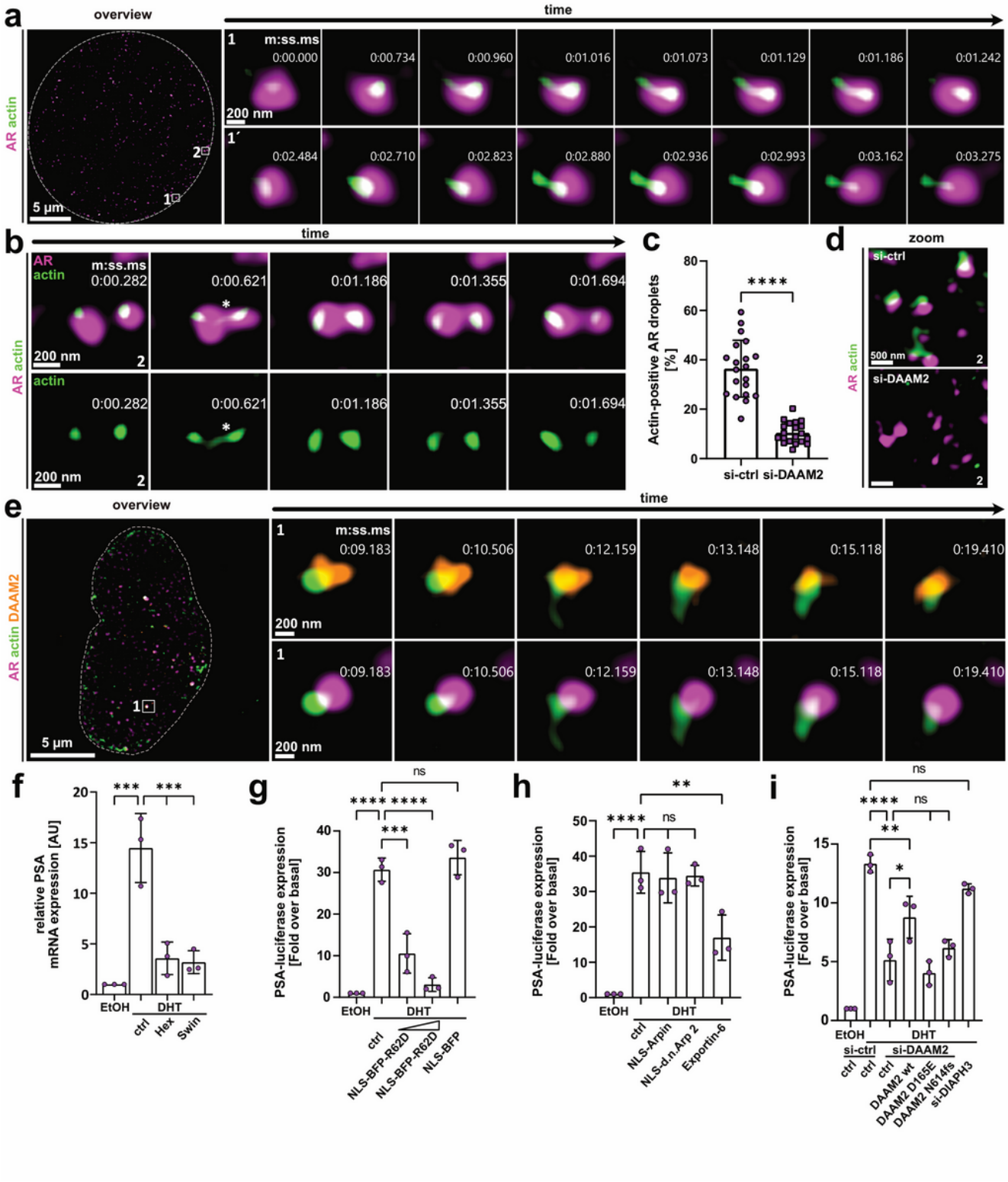

Figure 4

DHT signaling drives nuclear actin assembly at the AR by DAAM2. a SIM-burst mode timelapse video of NIH3T3 cell, stably expressing nuclear actin chromobody-mCherry transfected with AR-GFP (magenta) displaying nuclear actin tails at the AR after DHT-addition for 16 h; areas of zoom are indicated. **b** SIM-burst mode timelapse video of NIH3T3 cells showing fusion event of AR after DHT-signaling, indicated by white asterisks. **c** Quantification of actin-positive AR droplets of si-ctrl and si-DAAM2 treated NIH3T3 16 h

after DHT addition. Scatter dot bar plot showing single experiment values ± SD for 20 cells per condition in 3 biological replicates. **d** Representative zoom images for si-ctrl and si-DAAM2 treated NIH3T3 cells analyzed in (**c**), showing actin-positive AR droplets in control si-RNA treated cells. Overview is shown in Extended Data Fig. 3b. **e** SIM-burst mode timelapse video of LNCaP cells transfected with AR-GFP (magenta), DAAM2-mScarlet (orange) and nAC-SNAP (green) and stimulated with DHT for 16 h, showing DAAM2 mediated nuclear actin assembly. **f** qPCR-results for PSA gene expression after stimulation with EtOH or DHT and following treatments with Hexanediol or Swinholide in LNCaP cells. **g, h** PSA gene reporter assays in LNCaP cells transfected with either NLS-BFP-actin R62D and NLS-BFP (**g**) or NLS-Arpin, NLS-d.n.Arp2 or Exportin-6 (**h**) 24 h after DHT signaling. **i** PSA gene reporter assay in LNCaP cells 48 h after si-RNA treatment and re-expression of si-RNA resistant DAAM2. Scatter dot bar plot showing single experiment values ± SD in 3 independent biological replicates (**f-i**).

Supplementary Files

This is a list of supplementary files associated with this preprint. Click to download.

- rawdataDAAM2ARPolII.xlsx
- rawdataDAAM2andARdroplets.xlsx
- rawdataNIH3T3siDAAM2actinpositivedroplets.xlsx
- rawdataPSAreporterassaysLNCaP.xlsx
- rawdataqPCRLNCaP.xlsx
- rawdataWBanalysis.xlsx
- Supplementaryvideo1.mp4
- Supplementaryvideo2.mp4
- Supplementaryvideo3.mp4
- Supplementaryvideo4.mp4
- Supplementaryvideo5.mp4
- Supplementaryvideo6.mp4
- Supplementaryvideo7.mp4
- SupplementaryFig.1.pdf
- ExtendedDataFig.1.tif
- ExtendedDataFig.2.tif
- ExtendedDataFig.3.tif
- Additionalinformation.docx